Risk-Aware Fast Trajectory Planner for Uncertain Environments Based on Probabilistic Surrogate Reliability and Risk Contours

Guobiao Wang[1]

***Abstract*— This paper presents the risk-aware fast trajectory planner (RAFTER) for autonomous vehicles in dynamic uncertain environments, which is based on the probabilistic surrogate reliability of other traffic participants and risk contours. In contrast to the conventional risk metric, RAFTER not only provides the upper bound of the probability of constraint violation but deduces an infimum on the risk which the controlled plant can stand by the probabilistic reliable surrogate model. Such a risk-aware algorithm is capable of perceiving uncertainty and handling robustness. A series of covering disks are constructed utilizing a concise geometric configuration for a lower conservatism representation of the vehicle profile, which attains a desirable tradeoff between the quantity and area of occupation. Safe travel corridors are built on the dilated map via covering disks, significantly reducing the computational burden of a reliability-based optimization procedure for optimal trajectory planning. The effectiveness of the proposed method is confirmed by two numerical simulations derived from real scenarios.**

I. Introduction

While fast and efficient trajectory planners for static or dynamic environments have been extensively investigated in the literature [1], [2], a risk-aware trajectory one able to handle environmental uncertainties and surrogate imprecision remains an open problem.

With the development of intelligent connected vehicles (ICVs), risk-aware planning and control have received increasing attention, with some impressive works presented [3]–[13]. Addressing the inherent system uncertainties of the controlled plant, high order control barrier functions (HOCBFs) and control Lyapunov functions (CLFs) were combined to suppress the uncertainties of the model [7]. In [3], the upper and lower bounds of the risk were determined by the linear weighted sum of the moment for a clear indication of the probability of violation of safety constraints in the presence of bounded uncertainties. For the uncertainty of external obstacles, a risk management method called risk contours map was proposed to ensure probabilistic safety under perception uncertainties [5]. After the pioneering work [3], various concentration inequalities were developed to identify the upper bound of the probability of constraint violation, among which are Cantelli's inequality [9], one-sided Vysochanskij-Petunin inequality [11], and nonlinear Chebyshev's inequality [13]. However, the aforementioned risk contours are just based on the established models of other traffic participants without considering the surrogate reliability.

System reliability identification under insufficient and subjective data sets is crucial to any intelligent system [14], [15]. In the field of system safety and reliability engineering, various theoretically rigorous methodologies have turned up for obtaining probabilistic confidence intervals for system reliability [16]. However, the discussion on the risk metrics concerning surrogate reliability is insufficient. This work attempts to bridge the gap between the two. The trajectory planning problem is often constructed as an optimization one to solve. Under environmental risks and trustworthy probabilistic surrogates, optimization problems tend to be nonconvex and nonlinear. Reducing the solution complexity by designing some ingenious transformations for fast planning is a significant issue in such a context. Thereinto, the coverage of vehicle profiles and the construction of safe corridors have marked effects on setting an efficient planning framework.

Conventional covering elements include disks [2], rectangles [17] and hexagons [18]. Compared with the other two primitives, the disk representation has the following merits: (**i**) The distance from the center of mass of each disk to the boundary, i.e., the radius of disk r_d, is the same, which makes it convenient to dilate obstacles for the particle motion model of the ego vehicle; (**ii**) The disk representation is of less space complexity, storing only the three variables of $[\boldsymbol{x}_d, \boldsymbol{y}_d, r_d]$, where $\boldsymbol{x}_d$ and $\boldsymbol{y}_d$ denote the coordinates of the center of the disks. Nevertheless, the other two need to store at least four or six coordinates of vertices, respectively. In [6], a series of disks was adopted to represent the traffic participants for verification of the validity of this idea. However, the ego-car is covered by an ellipse, which still has certain conservatism. For that sake, the disk is taken as the covering element here. The design of the disk geometry significantly affects the narrowness of the dilated map. To further reduce the conservatism of the covering approach, the least and minimum covering disks for rectangle-oriented vehicle profiles are obtained through geometric configuration.

Based on a non-conservative coverage of the vehicle profile, the safe corridor can be constructed to efficiently reduce the searching space with safety guaranteed [1], [2]. After acquiring a global path rapidly, the safe corridors make a series of polyhedrons around each sampling point on the coarse path. The ego vehicle is ensured to be collision-free within these polyhedrons. The constrained optimization is then performed within this corridor to obtain the final

[1]Guobiao Wang is with School of Automation, Southeast University, Nanjing, Jiangsu, 210096, China and Key Laboratory of Measurement and Control of Complex Systems of Engineering, Ministry of Education, Nanjing, Jiangsu 210096,China gbwang@seu.edu.cn

planning trajectory that meets the performance requirements. Safe corridors can effectively reduce the computational burden of constrained planning problems, especially in narrow environments. Obviously, different profile coverage may lead to entirely different safe corridors, so it is vital to design non-conservative and tractable profile coverage for desired safe corridors.

Here, a nonlinear programming procedure is proposed for safety-critical trajectory planning for autonomous vehicles in uncertain environments. Unlike the conventional risk metric approaches based on an accurate prediction model of other traffic participants, the probabilistic reliability of the surrogate model is tapped. A safer risk contour map is acquired by means of the risk perception mechanism. A low-conservative vehicle profile representation transforms the contour map into a dilated one and the ego vehicle into a particle model. A feasible but coarse global path is obtained for the particle model through a global planner on this dilated map. With the help of the geometric information of vehicle coverage disks, safe travel corridors are acquired around the global path. Then, nonlinear programming in the safe corridors secures the optimal collision-free trajectory. In fact, the proposed approach is not intended to supersede but to be on top of existing state-of-the-art methodologies for constructing risk-aware planning strategy by the risk metric and trajectory planning approaches. The overall schematic diagram of the proposed planning scheme is shown in Fig. 1. Compared with the existing literature, the main contributions of this work are summarized as follows:

1) A risk-aware trajectory planner is developed for autonomous vehicles in dynamic uncertain environments. In contrast to the conventional risk contour map, RAFTER bridges the gap between risk metric and probabilistic surrogate reliability.
2) A low conservative representation of the vehicle profile is obtained by constructing a series of covering disks, which ensures a desirable tradeoff between the quantity and area of occupation by concise geometric configuration.
3) An array of safe travel corridors is built on the dilated map via the covering disks. They significantly reduce the computational burden of nonlinear programming for optimal trajectory planning.

Notation: $\mathcal{U}(l_b, u_b)$, $\mathcal{N}(\mu, \sigma^2)$ and $\mathcal{B}(\alpha, \beta)$ denote the uniform distribution with minimum l_b and maximum u_b, the normal distribution with mean μ and variance σ^2, and the $Beta$ distribution with parameters α and β, respectively. $\underline{*}$ and $\overline{*}$ are the lower and upper bounds of the corresponding variable. $\mathbf{E}[*]$ is the expected value of the component.

II. Problem Statement

The concerned trajectory planning problem for uncertain environments is defined here. The kinematic principle of ego vehicle can be modeled by

$$\dot{\boldsymbol{s}} = f(\boldsymbol{s}, \boldsymbol{u}), \quad \text{for } t \in [t_0, t_f] \tag{1}$$

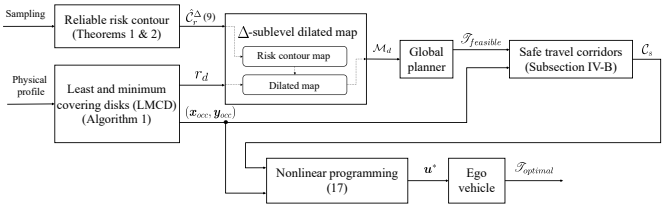

Fig. 1. Overall schematic diagram of proposed control scheme.

where t_0 and t_f refer to the start and terminal timestamps of the planning procedure, the state profiles and control profiles are vectorized as $\boldsymbol{s} = [x, y, \theta, v, \phi]^\top$ and $\boldsymbol{u} = [a, \omega]^\top$, $(x, y) \in \mathcal{X}$ is the position of the ego vehicle's rear-axle midpoint in the Cartesian coordinate frame, θ, v, a, ϕ and ω denote the yaw angle, longitudinal velocity, acceleration, steering angle and angular velocity, respectively.

For the planning task with the desired destination, the planning procedure of the ego vehicle should comply with the following constraints to ensure task completion and safety.

1) Two-point boundary constraints
$$\boldsymbol{s}(t_0) = \boldsymbol{s}(0) \quad \text{and} \quad \boldsymbol{s}(t_f) = \boldsymbol{s}_{target} \tag{2}$$
where $\boldsymbol{s}(0)$ and $\boldsymbol{s}_{target}$ are the initial and target states of the ego vehicle.
2) External obstacle avoidance constraints
All traffic participants can be represented by polygons $\mathcal{V}$, including ego vehicle $\mathcal{V}_{ego}$, other traffic participants and obstacles $\mathcal{V}_{obs}$. The constraint can be expressed as
$$\mathcal{V}_{ego}(t) \cap \mathcal{V}_{obs_i}(t) = \emptyset, \quad \forall t \in [t_0, t_f] \tag{3}$$
where $i = \{1, 2, ..., n_o\}$, and n_o is the total number of other traffic participants and obstacles. It should be noted that the polygon is not suitable for planning in complex environments though the representation of the ego vehicle as a polyhedron is intuitive. An alternative representation of vehicles for higher efficiency is presented in subsection IV-A.
3) Kinematic constraints
The concerned kinematic components are set as $\boldsymbol{s}_1 = [a, v, \omega, \phi]^\top$, and the boundary constraint is
$$\boldsymbol{s}_1 \in [\underline{\boldsymbol{s}_1}, \overline{\boldsymbol{s}_1}], \quad \forall t \in [t_0, t_f] \tag{4}$$

The cost function J indicates the performance indexes that are of interest to the planning task, which can be defined as

$$J = \sum_{i=1}^{n_J} w_i J_i \tag{5}$$

where J_i is the performance index component, such as the traverse time or comfortable capability; n_J is the number of concerned indexes; w_i is the weight of the corresponding component.

Then the concerned planning task can be formulated by the following optimal control problem:

$$\boldsymbol{u}^* = \arg\min_{\boldsymbol{u}} (5) \quad s.t. \text{ Conditions } (1) - (4) \tag{6}$$

In general, the two-point boundary conditions (2) and kinematic constraints (4) are deterministic. The disturbance of ego vehicle (1) can be suppressed effectively by robust control [17] or adaptive control [19]. Then (6) can be succinctly solved by a plethora of existing mature optimization solvers, provided that the external obstacles are accurately represented. However, no approach so far can confidently claim the perfect modeling accuracy of other traffic participants, especially the ones based on data-driven prediction. Inaccurate scenario modeling will degrade trajectory planning performance or give even unsafe results. In the present study, imperfection is allowed in the prediction module but with explicit knowledge of the risk level. Within this context, we focus on solving (6) correctly to ensure safe decision-making and planning of autonomous vehicles in uncertain environments under imprecise scenario modeling.

III. Reliable risk contour

Inspired by [6], [8], [9], [11], the construction of risk contour here adopts the same notations and definitions from these papers. Within this context, the risk contour is extended to the uncertain traffic participants and the probabilistically reliable surrogate model simultaneously in this section. The boundary of the risk contour is derived in subsection III-A. Then an illustrative example is demonstrated to visualize the theoretical results in subsection III-B.

A. Reliable risk contour

Traffic participants and scene occupation are taken here as obstacles for brevity. The uncertain obstacles are given by

$$\mathcal{V}_{obs_i} = \{\boldsymbol{x} \in \mathcal{X} : P_i(\boldsymbol{x}, \xi_i, t) \geq 0\} \tag{7}$$

where $i = \{1, 2, ..., n_o\}$, $t \in [t_0, t_f]$, $\boldsymbol{x} := (x, y)$, ξ is the uncertain component, and P_i denotes the surrogate model of the i-th obstacle. When there is no component t in the suurrogate P_i, the i-th obstacle is taken to be static, and the opposite is true for dynamic obstacles.

It is noteworthy that P in (7) is assumed to be reliable with a reliability indicator $r_i \in [0, 1]$. Then the unreliability indicator can be obtained by $r_s = 1 - r_i$. The harmonic mean of precision and recall, i.e., F1-score, is used to characterize the reliability indicator r_i. Arbitrary state-of-the-art prediction approaches are supposed to be capable of securing the surrogate model P. Recommended here are surrogates with analytic expressions such as mixed Gaussian process and polynomials for easy acquisition of the required moment information. Substituting (7) into (3) turns the original obstacle avoidance constraints into chance constraints. It is impractical to directly solve the optimization problem (6) subject to the coupling uncertainty. Against this backdrop, this section aims to get (3) in a tractable form. To achieve this aim, risk contour is introduced as below:

Definition 1: Risk Contours [5], [9], [11]: Given the acceptable risk level $\Delta \in [0, 1]$, the $\Delta-$sublevel risk contour represents the set of all points in the environment whose risk is less or equal to Δ, and can be defined as

$$\mathcal{C}_r^{\Delta}(t) := \{\boldsymbol{x} \in \mathcal{X} : \mathscr{P}(\boldsymbol{x} \in \mathcal{V}_{obs}(\xi, t)) \leq \Delta\} \tag{8}$$

where $\mathscr{P}$ is the probability distribution function. The main idea is to construct the risk contour via (8) so as to transform the chance constraint (3) into a deterministic one only in terms of $\boldsymbol{x}$. The following theorem yields the risk contour:

Theorem 1: Consider the surrogate model $P(\boldsymbol{x}, \xi_i, t)$ of the uncertain obstacle with the unreliability indicator $r_s \in [0, 1]$. The following set $\hat{\mathcal{C}}_r^{\Delta}(t)$ is an inner approximation of the risk contour $\mathcal{C}_r^{\Delta}(t)$ in (8) [8], [9]:

$$\hat{\mathcal{C}}_r^{\Delta}(t) = \left\{\boldsymbol{x} \in \mathcal{X} : 1 - \frac{(1 - r_s)^2 * \mathbf{E}[P(\boldsymbol{x}, \xi, t)]^2}{\mathbf{E}\left[P^2(\boldsymbol{x}, \xi, t)\right]} \leq \Delta\right\} \tag{9}$$

where $\mathbf{E}[P(\boldsymbol{x}, \xi_i, t)]$ and $\mathbf{E}[P^2(\boldsymbol{x}, \xi_i, t)]$ denote the expectation and the variance of $P(\boldsymbol{x}, \xi_i, t)$.

Proof: Since $\mathscr{P}(\boldsymbol{x} \in \mathcal{V}_{obs}(\xi, t)) = \mathscr{P}\{P(\boldsymbol{x}, \xi_i, t) \geq 0\}$, solving the chance constraint (8) is equivalent to finding an upper bound for the tail probability in the distribution of $P(\boldsymbol{x}, \xi_i, t) \geq 0$. Using the similar arguments as those of Theorem 1 in [8], [9], the upper bounds for the multivariate tail probability can be deduced by the folllowing *Paley-Zygmund inequality*-like boundary condition [20]:

$$\mathscr{P}(P > r_s \mathbf{E}[P]) \leq 1 - \frac{(1 - r_s)^2 * \mathbf{E}[P]^2}{\mathbf{E}\left[P^2\right]} \tag{10}$$

Inserting (10) into (8) gives (9). Thus, the risk contour under the probabilistic reliable surrogate addressing the nonconvex and nonlinear sets of obstacles can be acquired. ■

Remark 1: If the surrogate model is fully trusted, i.e., $r_s = 0$, then (10) reduces to the *Cantelli's inequality* based on higher-order moment information in [9]. However, if it is considered totally unreliable, i.e. $r_s = 1$, then $\mathscr{P}(P > 0) \leq 1$ always holds. That is to say, the controlled plant is under an extremely dangerous decision-making mechanism. In general, the prior knowledge about the trustworthiness of the surrogate model is taken into account in risk modeling, which endows the controlled system with a higher degree of safety guarantee for uncertain environments.

The following theorem is to deduce the lower bound of risk that the controlled plant can secure under the probabilistic trusted surrogate of other traffic participants.

Theorem 2: Consider the surrogate model $P(\boldsymbol{x}, \xi_i, t)$ of the uncertain obstacle with a unreliability indicator $r_s \in [0, 1]$. The lower bound of risk that the controlled plant can secure is formulated by

$$\underline{\mathcal{C}_r} = \left\{\boldsymbol{x} \in \mathcal{X} : \frac{(2r_s - r_s^2) * \mathbf{E}[P(\boldsymbol{x}, \xi, t)]^2}{\mathbf{E}\left[P^2(\boldsymbol{x}, \xi, t)\right]}\right\} \tag{11}$$

Proof: If the surrogate model is fully trustworthy, i.e., $r_s = 0$, (10) reduces to

$$\mathscr{P}(P > 0) \leq \frac{\mathbf{E}\left[P^2\right] - \mathbf{E}[P]^2}{\mathbf{E}\left[P^2\right]} \tag{12}$$

Removing (12) from (10) yields

$$1 - \frac{(1 - r_s)^2 * \mathbf{E}[P]^2}{\mathbf{E}\left[P^2\right]} \geq \frac{(2r_s - r_s^2) * \mathbf{E}[P]^2}{\mathbf{E}\left[P^2\right]} \tag{13}$$

which indicates that the infimum of risk (10) is $\max\{\frac{(2r_s - r_s^2) * \mathbf{E}[P]^2}{\mathbf{E}[P^2]}\}$. ■

B. Illustrative example

An illustrative example is provided here to demonstrate the results of Theorems 1 and 2.

Consider the state region $\mathcal{X} \in [-1,1]^2$. The uncertain obstacle is described by the polynomial $P(\boldsymbol{x},\boldsymbol{\xi}) = 0.081 * x_1 - 0.04104 * \xi_2 - 0.25 * \xi_1 - 0.342 * x_2 + 0.495 * x_1 * \Xi_1 - 0.522 * x_1 * \Xi_1^2 + 1.233 * x_1^2 * \Xi_1 + 0.126 * x_1 * \Xi_1^3 - 0.423 * x_1^3 * \Xi_1 + 0.261 * x_1 * \Xi_1^4 - 0.792 * x_1^4 * \Xi_1 - 0.585 * \Xi_1^2 + 0.612 * \Xi_1^3 - 0.324 * \Xi_1^4 - 0.081 * \Xi_1^5 - 0.063 * x_1^2 * \Xi_1^2 - 0.585 * x_1^2 * \Xi_1^3 + 0.27 * x_1^3 * \Xi_1^2 + 0.108 * x_1^2 - 0.054 * x_1^3 - 0.261 * x_1^4 - 0.009 * x_1^5 + 0.104$, where $\Xi_1 = 0.12 * \xi_2 + x_2$, $\xi_1 \sim \mathcal{N}(0.1, 0.001)$ and $\xi_2 \sim \mathcal{B}(12,1)$. The risk threshold $\Delta = 0.3$ and the unreliability indicator of surrogate $P(\boldsymbol{x},\boldsymbol{\xi})$ is $r_s = 0.1$.

Fig. 2 gives the reliable risk contour derived by (9) under the model unreliability $r_s = 0.1$. Comparison of risk sets with and without model reliability at $\Delta = 0.3$ is illustrated in Fig. 3. As shown in Fig. 2, the risk threshold under model reliability $1 - r_s = 0.9$ rises to $\max\{\frac{(2r_s - r_s^2) * \mathbf{E}[P]^2}{\mathbf{E}[P^2]}\}$, i.e., the infimum of risk. That is to say, the risk of the controlled plant in the current uncertain environment is no less than $\max\{\frac{(2r_s - r_s^2) * \mathbf{E}[P]^2}{\mathbf{E}[P^2]}\}$, provided that the surrogate model of other participants has an unreliability of $r_s = 0.1$.

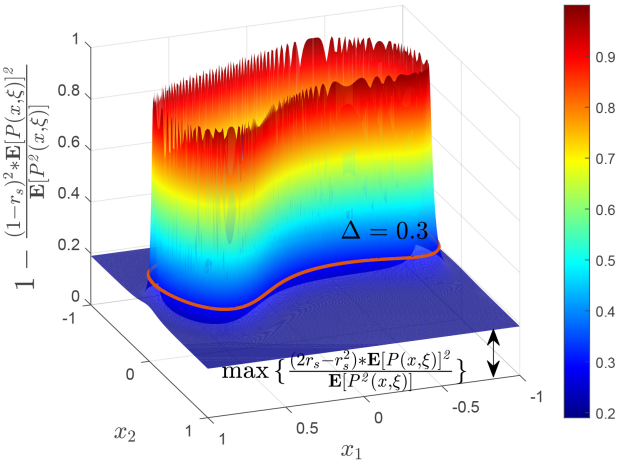

Fig. 2. Reliable risk contour derived by (9) upon $r_s = 0.1$.

IV. Safety-Critical Trajectory Planning Framework

As demonstrated by Fig. 3, stressing model reliability narrows the feasible region. Thus an optimal tractable control framework is designed for safe trajectory planning in such narrow environments. In subsection IV-A, geometric configuration is introduced to determine the occupation of the vehicle with low conservatism. Construction of the safe travel corridor for ego vehicle is presented in subsection IV-B. A more desirable trajectory planning framework than (6) is provided in subsection IV-C.

A. Least and minimum covering disks

Least and minimum covering disks (LMCD) of the ego vehicle are obtained via the geometric configuration. Secured

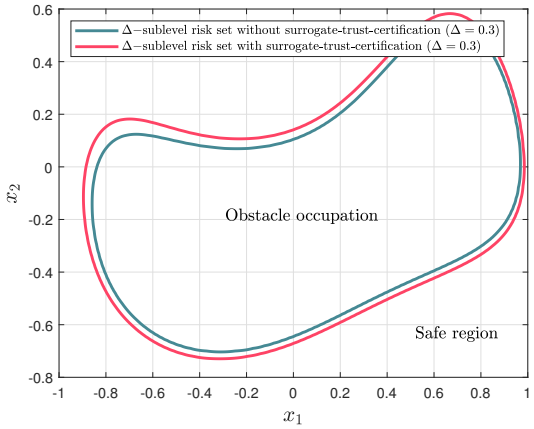

Fig. 3. Comparison of risk sets with and without model reliability upon $\Delta = 0.3$ and $r_s = 0.1$.

first is the LMCD representation of the ego vehicle placed horizontally and then rotated by θ radians with the midpoint of its rear suspension for its non-conservative coverage at any position in the scene.

Assume that the parameters of the profile are known, including the front overhang length L_f, vehicle wheelbase L_w, rear overhang length L_r, vehicle width C_w and rear suspension midpoint (x_r, y_r). Then the boundary of the ego vehicle placed horizontally can be written as

$$\begin{aligned} x_{c_l} &= x_r - \mathrm{L}_r, \quad x_{c_u} = x_r + \mathrm{L}_w + \mathrm{L}_f \\ y_{c_l} &= y_r - \mathrm{C}_w/2, \quad y_{c_u} = y_r + \mathrm{C}_w/2 \end{aligned} \tag{14}$$

where x_{c_l}, x_{c_u}, y_{c_l} and y_{c_u} denote the upper and lower bounds of the ego vehicle placed horizontally in the cartesian coordinate, reapectively. The radius of the minimum covering disk is set as

$$r_d = \frac{\sqrt{2}\mathrm{C}_w}{2} \tag{15}$$

The corresponding y-coordinate vector is the one with the same length $\boldsymbol{x}_d$ and all elements y_r. Then each disk is rotated with (x_r, y_r) as the center and θ radians as the rotation angle to obtain the actual occupancy $(\boldsymbol{x}_{occ}, \boldsymbol{y}_{occ})$ of ego vehicle. The pseudocode for LMCD is given in Algorithm 1. Fig. 4 shows the LMCD representation for four different vehicle profiles. It can be seen that LMCD can adaptively give less conservative coverage representation of different profiles. More importantly, as a lightweight representation procedure, LMCD has great potential for other planning algorithms that require the online representation of various traffic participants.

B. Safe travel corridors

With the least and minimum covering disks obtained in subsection IV-A, safe travel corridors can be built to ensure the safety of the planned trajectory and reduce the computational burden of the planning procedure. Construction of the corridors under LMCD representation of ego vehicle falls into the following steps:

Algorithm 1: Least and minimum covering disks (LMCD)

Input: the front overhang length L_f, vehicle wheelbase L_w, rear overhang length L_r, vehicle width C_w, and rear suspension midpoint (x_r, y_r);

Output: The center of the covering disk $(\boldsymbol{x}_{occ}, \boldsymbol{y}_{occ})$, the radius of the covering disk r_d;

Initialization: $i = 1$;
% Least and minimum covering disks;
Calculate the boundary of ego vehicle placed horizontally x_{c_l}, x_{c_u}, y_{c_l} and y_{c_u} (14);
Determine the minimum radius of the covering disk (15);
while $x_{c_u} - (x_r - \mathrm{L}_r + \mathrm{C}_w/2 + (i-1)\mathrm{C}_w) > \mathrm{C}_w/2$ **do**
    Determine the x-coordinate of the center of the i-th disk $x_{d_i} = x_{c_l} + \mathrm{C}_w/2 + (i-1)\mathrm{C}_w$;
    $i = i + 1$;
end
if $x_r - \mathrm{L}_r + \mathrm{C}_w/2 + (i-1)\mathrm{C}_w \neq x_{c_u}$ **then**
    $x_{d_i} = x_r + \mathrm{L}_w + \mathrm{L}_f - \mathrm{C}_w/2$;
end
Determine the y-coordinate of the center of the i-th disk;
% Rotation;
for $j = 1 : length\{x_d\}$ **do**
    $\boldsymbol{x}_{occ} = x_r + (x_{d_j} - x_r)\cos\theta - (y_{d_j} - y_r)\sin\theta$;
    $\boldsymbol{y}_{occ} = y_r + (x_{d_j} - x_r)\sin\theta + (y_{d_j} - y_r)\cos\theta$;
end
return $\boldsymbol{x}_{occ}$, $\boldsymbol{y}_{occ}$ and r_d.

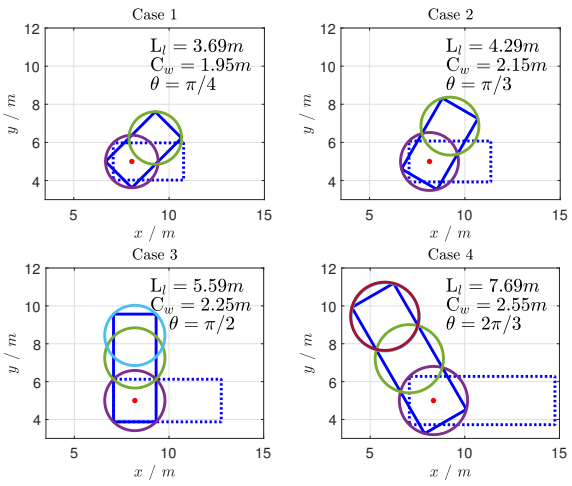

Fig. 4. LMCD representation for four different vehicle profiles.

step 1. Convert the environmental obstacles into dilated ones by the indicator r_d in (15), and then acquire the dilated environmental map $\mathcal{M}_d$;
step 2. The midpoint of rear suspension is taken as the particle to be controlled, and a feasible path $\mathscr{T}_{feasible} := (\boldsymbol{x}_{feasible}, \boldsymbol{y}_{feasible})$ is secured via the global planner under the dilated environmental map $\mathcal{M}_d$;
step 3. Combined with the feasible trajectory $\mathscr{T}_{feasible}$ and the physical profile of the ego vehicle, the travel trajectory $\mathscr{T}_d$ of each covering disk is obtained;
step 4. Construct safe corridors $\mathcal{C}_s$ for each travel trajectory $\mathscr{T}_{d_i}$ by specific rules.

Step 1 gives a simple geometric transformation. Step 2 can be realized by mature global planning algorithms, e.g., A*, hybrid A* and RRT*. Step 3 is critical as it directly affects the construction of the corridors. Step 4 involves some effective construction rules [2]. In this study, hybrid A* is taken to build the coarse global path in Step 2 and Algorithm 2 in [2] is adopted to generate the travel corridors in Step 4. It is worth noting that with the feasible path of the rear suspension midpoint well planned, the motion trajectory of each disk in Step 3 can be conveniently identified based on the LMCD representation. In particular, if we set $x_{r_k} = x_{feasible_k}$ and $y_{r_k} = y_{feasible_k}$, with x_{d_i} and θ_k already confirmed, the travel trajectory of each covering disk $\mathscr{T}_{d_i}$ can be easily determined by lines $14-17$ of Algorithm 1, where $i = \{1, 2..., n_d\}$, n_d denotes the number of discs , and k is the number of discrete points on $\mathscr{T}_{feasible}$.

C. Tractable nonlinear programming

Based on the above, a tractable nonlinear programming framework is proposed for safe trajectory planning in uncertain environments. Compared with the conventional optimal control problem (6), the main difference is that the obstacle avoidance constraints addressed in this work take into account the environmental uncertainties and the reliability of the surrogate.

In Section III, Theorem 1 defines an upper bound on the collision probability for the obstacles with uncertainties and their surrogates with probabilistic reliability. Theorem 2 gives a lower bound on the risk that the ego vehicle may encounter under probabilistic reliability of the obstacle surrogate model. In other words, Theorem 1 determines the region of probabilistic safety under environmental uncertainties, and Theorem 2 quantifies the risk perception of the environment. By Algorithm 1, we can acquire the less conservative representation of the ego vehicle. Combining the risk contour $\hat{\mathcal{C}}_r^{\Delta}$ derived from Theorem 1 with the radius of the minimum coverage circle r_d deduced from Algorithm 1, we obtain the dilated map $\mathcal{M}_d$, with the help of which the safe travel corridors $\mathcal{C}_s$ can be secured by taking Steps 2-4 mentioned above. Then the ego vehicle only needs to execute a nonlinear programming procedure in the corridors for an optimal safety trajectory. In this case, the external obstacle avoidance constraints (3) and chance constraints (8) are converted to the following deterministic constraints:

$$\boldsymbol{x}_{ego} \in \mathcal{C}_s \tag{16}$$

Compared to the optimal control problem (6) on the global map, the proposed tractable nonlinear programming framework greatly reduces the search domain for optimization and ensures probabilistic safety in the uncertain environment. And it is formulated as follows:

$$\min_{\boldsymbol{u}} \quad \text{Cost function (5)} \tag{17a}$$

subject to

$$\text{Kinematic model (1)} \tag{17b}$$

$$\text{Boundary conditions (2)} \tag{17c}$$

$$\text{Kinematic constraints (4)} \tag{17d}$$

$$\text{Obstacle avoidance constraints (16)} \tag{17e}$$

V. Experimental results and discussions

In this section, the performance of the proposed safety-critical trajectory planning framework is demonstrated via the numerical simulations of two typical scenarios, i.e., on-road cut-in in subsection V-A and automatic parking in a narrow environment in subsection V-B. The nonlinear programming problem is solved by an open-source NLP solver called IPOPT [21] in the MATLAB+AMPL environment [22]. The simulations presented were carried out on Desktop PC with an Intel Core $i7-7700$ HQ processor with 3.20 GHz and 16.0 GB RAM, running on Windows 10 Enterprise.

A. On-road cut-in

Cut-in is a common scenario for autonomous on-road driving, requiring higher risk control ability than adaptive cruise control (ACC) [23], [24]. This section explores the maneuverability of the proposed strategy for rear-end risk avoidance.

The kinematic principle of the ego vehicle is modeled here as the well-known bicycle model [25]. Its basic parameters are set as: the front overhang length $\mathrm{L}_f = 0.96\ m$, vehicle wheelbase $\mathrm{L}_w = 2.80\ m$, rear overhang length $\mathrm{L}_r = 0.929\ m$, vehicle width $\mathrm{C}_w = 1.942\ m$, and the upper bound of concerned kinematic components are $\boldsymbol{s}_{1_{max}} = [a_{max}, v_{max}, \omega_{max}, \phi_{max}]^\top = [5.0\ m/s^2, 10.0\ m/s, 1.50\ rad, 0.85\ rad/s]^\top$. This scenario has two dynamic traffic participants, whose surrogate models are given by $P = \xi_1^2 - \frac{(x-p_x)^2}{(\alpha_1 \mathrm{C}_w)^2} - \frac{(y-p_y)^2}{(\alpha_1 \mathrm{L}_l)^2}$, where $\mathrm{L}_l = \mathrm{L}_f + \mathrm{L}_w + \mathrm{L}_r$, $p_x = \hat{x} + \alpha_2 \xi_2$, $p_y = \hat{y} + \alpha_3 \xi_3$, $\hat{x}$ and $\hat{y}$ denote the smooth estimated trajectories, $\alpha_1 = 1.2$, $\alpha_2 = 0.2$, $\alpha_3 = 0.1$, $\xi_1 \sim \mathcal{U}(0.3, 0.4)$, $\xi_2 \sim \mathcal{N}(0, 0.1)$, and $\xi_3 \sim \mathcal{B}(3, 4)$. The desired risk upper bound on probability is $\Delta = 0.1$, and the unreliability indicator of surrogate $r_s = 0.05$. The concerned performance indexes include the traverse time t_t and the jerk j_e. The cost function can be written as $J_{E01} = w_1 t_t + w_2 j_e^2$, where $w_1 = w_2 = 0.5$.

Fig. 5 demonstrates the optimized trajectory footprints derived by nonlinear programming (17). A distance comparison between the ego vehicle and the ahead one after a successful cut-in maneuver with or without reliability-aware is given in Fig. 6, which shows that the terminal distance of the reliability-aware maneuver derived by (17) is $1.208\ m$, while that without reliability-aware is 0.7522. In general, the proposed approach promises more reliable rear-end risk-avoidance maneuvers.

B. Automatic parking

In contrast to the on-road planner generally working in a structured scenario, a parking-oriented one is capable of handling more complex situations. On the one hand, the space available in the parking lot is relatively narrow, and on the other, static/dynamic obstacles may turn up anytime due to restricted visibility [25]. That makes the safety-critical decision-making and planning require both desirable real-time performance and timely risk awareness.

Considered here is the parking scenario with eight parked vehicles and one uncertain participant. The vehicles of different profiles are parked in a heterogeneous manner. The planning procedure is divided into two segments by the three specific timestamps: the initial moment t_0, the replanning moment t_r and the terminal moment t_f. The ego vehicle $\mathcal{V}_{ego}$ detects the sudden environmental changes at t_0, and the obstacle profile is recorded as P_{t_0}, from which $\mathcal{V}_{ego}$ derives an initial planning trajectory $\mathscr{T}_{initial}$. In the time horizon $t \in [t_0, t_r]$, $\mathcal{V}_{ego}$ runs along $\mathscr{T}_{initial}$ and collects the sampling information of an uncertain obstacle, and constructs its surrogate model. Then it obtains a replanned risk-aware trajectory at t_r by executing nonlinear planning (17) till the terminal timestamp t_f. The desired risk upper bound on probability is $\Delta = 0.1$ and the unreliability indicator of surrogate $r_s = 0.03$. The concerned performance indexes include the traverse time t_t and the jerk j_e. The cost function can be written as$J_{E01} = w_1 t_t + w_2 j_e^2$ with $w_1 = w_2 = 0.5$. The uncertain participant is formulated by $P = \xi_1^2 - \frac{(x-p_x)^2}{\alpha_1^2} - \frac{(y-p_y)^2}{\alpha_2^2}$ with $p_x = \hat{x} + \alpha_3 \xi_2$ and $p_y = \hat{y} + \alpha_7 \xi_3$, where $\alpha_1 = 2.0$, $\alpha_2 = 5.2$, $\alpha_3 = 0.2$, $\alpha_7 = 0.1$, $\xi_1 \sim \mathcal{U}(0.2, 0.3)$, $\xi_2 \sim \mathcal{N}(0, 0.01)$, and $\xi_3 \sim \mathcal{B}(3, 3)$.

Fig. 7 illustrates the footprints of initial planned trajectory without risk-aware at time step t_0. After sampling the uncertain environmental changes and representing ego vehicle $\mathcal{V}_{ego}$ with a series of covering disks, the corresponding safe travel corridors $\mathcal{C}_s$ are built as shown in Fig. 8. Based on the corridors, the replanned trajectory with risk-aware is obtained as shown in Fig. 9. Fig. 10 compares the planned trajectories with three different strategies: the initial planned trajectory without risk-aware, the online planned trajectory via real-time detection and the replanned trajectory with risk-aware. As indicated by Fig. 10, the proposed planning strategy manages to swiftly plan a probabilistically safe trajectory in a narrow scenario, much safer than the conventional optimal control-based approach (6), more efficient and comfortable than the real-time control. The comparative simulation results are given in Table I considered some fiducial performance indicators.

VI. Conclusion

A risk-aware fast trajectory planner for autonomous vehicles operating in uncertain environments has been developed. RAFTER focuses on the probability reliability of surrogates instead of the exact models of other traffic participants,

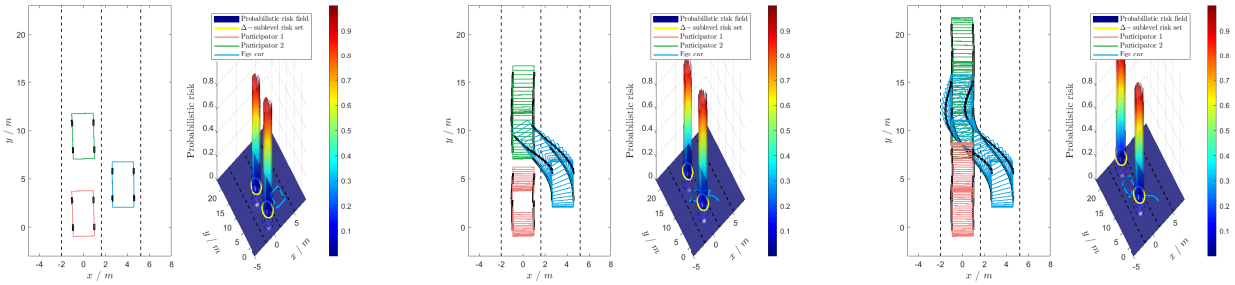

(a) $t = 0\ s$ (b) $t = 3.7327\ s$ (c) $t = 7.4654\ s$

Fig. 5. Optimized trajectory and footprints derived by nonlinear programming (17)

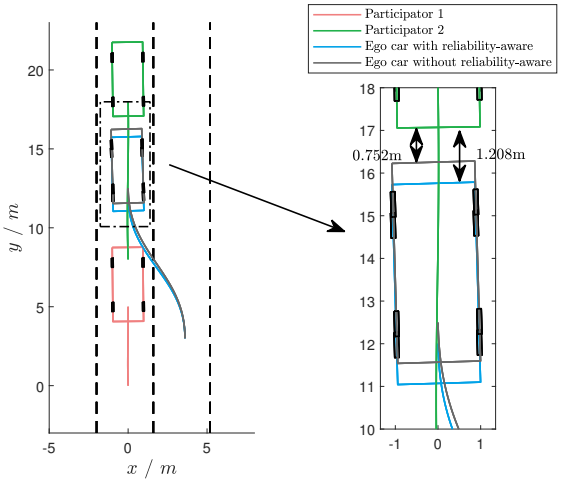

Fig. 6. Distance comparison between ego vehicle and ahead one after successful cut-in maneuver

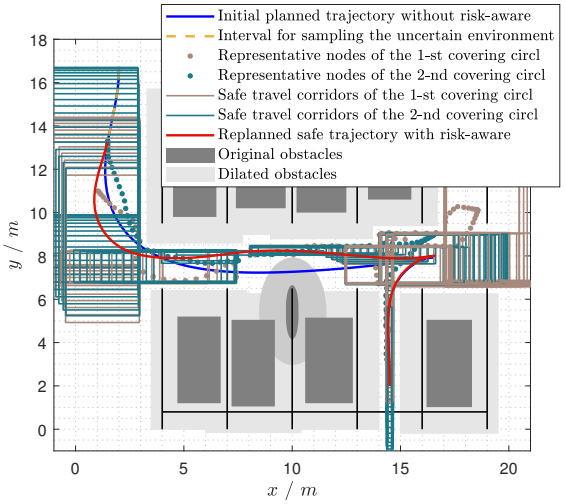

Fig. 8. Safe travel corridors of covering disks.

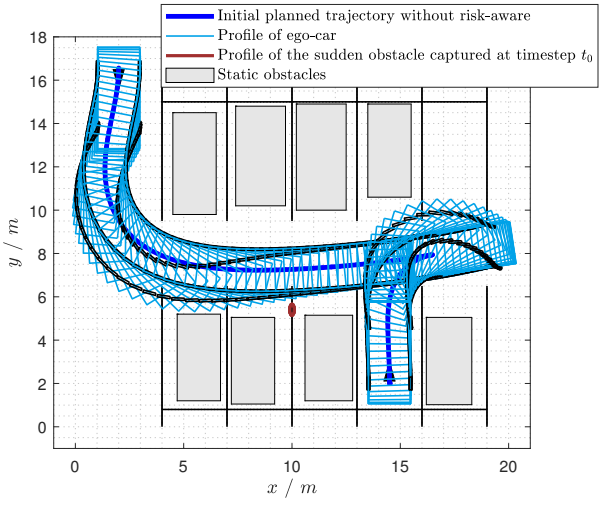

Fig. 7. Footprints of initial planned trajectory without risk-awarer at time step t_0.

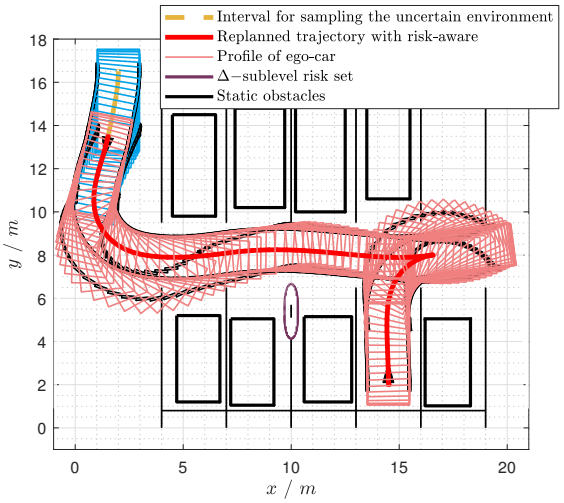

Fig. 9. Footprints of replanned trajectory with risk-awarer at time step t_r.

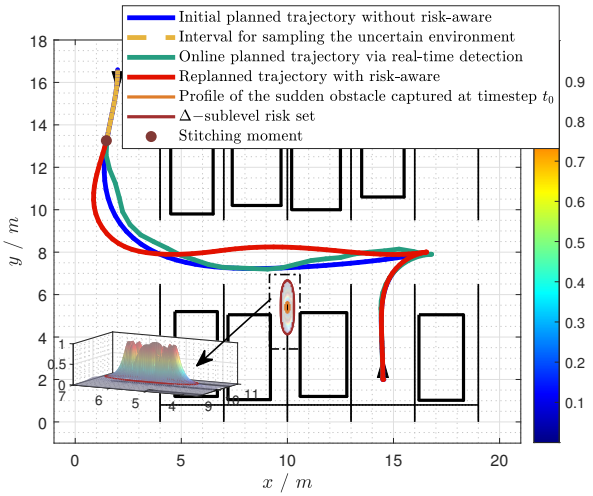

Fig. 10. Comparison of planned trajectories among three different strategies.

TABLE I

PERFORMANCE COMPARISON OF DIFFERENT CONTROL STRATEGIES

Indicator	OCP (6)	Online OCP	NLP (17)
t_{cpu} (sec)	12.142	385.26	**5.620**
I_c	**0.885**	1.135	0.893
S_r (%)	55.0	95.3	**100**

[1] t_{cpu}, $I_c = \sqrt{\frac{\sum_{i=1}^{N_t} j_{e_i}^2}{N_t}}$ and $S_r = \frac{N_s}{N_E}$ denote the average CPU running time, comfort index and success rate, where j_e denotes the jerk, N_t is the actual sampling times of the control input $\boldsymbol{u}$, N_s represents the number of successful runs and N_E is the total number of repeated experiments (herein set as $N_E = 300$).

[2] The optimal results are shown in bold.

which conventional strategies rely upon. Theoretical derivation provides the upper bound of the probability of constraint violation and an infimum on the risk that the controlled plant can handle in an uncertain environment. As confirmed by the experimental results, the proposed method promises safer risk-avoidance maneuvers and rapid trajectory replanning for sudden environmental changes, which ensures a desirable trade-off between safety and real-time performance. Future work is expected to extend the results to networked multi-agents and hardware experiments.

ACKNOWLEDGMENT

The author would like to thank Professor Lu Li for his valuable comments and suggestions.

REFERENCES

[1] J. Tordesillas, B. T. Lopez, M. Everett, and J. P. How, "Faster: Fast and safe trajectory planner for navigation in unknown environments," *IEEE Transactions on Robotics*, 2021.

[2] B. Li, T. Acarman, Y. Zhang, Y. Ouyang, C. Yaman, Q. Kong, X. Zhong, and X. Peng, "Optimization-based trajectory planning for autonomous parking with irregularly placed obstacles: A lightweight iterative framework," *IEEE Transactions on Intelligent Transportation Systems*, 2021.

[3] A. M. Jasour, A. Hofmann, and B. C. Williams, "Moment-sum-of-squares approach for fast risk estimation in uncertain environments," in *2018 IEEE conference on decision and control (CDC)*. IEEE, 2018, pp. 2445–2451.

[4] C. Hubmann, J. Schulz, M. Becker, D. Althoff, and C. Stiller, "Automated driving in uncertain environments: Planning with interaction and uncertain maneuver prediction," *IEEE transactions on intelligent vehicles*, vol. 3, no. 1, pp. 5–17, 2018.

[5] A. M. Jasour and B. C. Williams, "Risk contours map for risk bounded motion planning under perception uncertainties." in *Robotics: Science and Systems*, 2019.

[6] A. Wang, A. Jasour, and B. C. Williams, "Non-gaussian chance-constrained trajectory planning for autonomous vehicles under agent uncertainty," *IEEE Robotics and Automation Letters*, vol. 5, no. 4, pp. 6041–6048, 2020.

[7] W. Xiao, C. G. Cassandras, and C. A. Belta, "Bridging the gap between optimal trajectory planning and safety-critical control with applications to autonomous vehicles," *Automatica*, vol. 129, p. 109592, 2021.

[8] A. Jasour, W. Han, and B. Williams, "Real-time risk-bounded tube-based trajectory safety verification," in *2021 60th IEEE Conference on Decision and Control (CDC)*. IEEE, 2021, pp. 4307–4313.

[9] ——, "Convex risk bounded continuous-time trajectory planning in uncertain nonconvex environments," 2021.

[10] F. S. Barbosa, B. Lacerda, P. Duckworth, J. Tumova, and N. Hawes, "Risk-aware motion planning in partially known environments," in *2021 60th IEEE Conference on Decision and Control (CDC)*. IEEE, 2021, pp. 5220–5226.

[11] W. Han, A. Jasour, and B. Williams, "Non-gaussian risk bounded trajectory optimization for stochastic nonlinear systems in uncertain environments," *IEEE International Conference on Robotics and Automation*, 2022.

[12] X. Tang, K. Yang, H. Wang, J. Wu, Y. Qin, W. Yu, and D. Cao, "Prediction-uncertainty-aware decision-making for autonomous vehicles," *IEEE Transactions on Intelligent Vehicles*, vol. 7, no. 4, pp. 849–862, 2022.

[13] A. Jasour, X. Huang, A. Wang, and B. C. Williams, "Fast nonlinear risk assessment for autonomous vehicles using learned conditional probabilistic models of agent futures," *Autonomous Robots*, vol. 46, no. 1, pp. 269–282, 2022.

[14] L. Janson, T. Hu, and M. Pavone, "Safe motion planning in unknown environments: Optimality benchmarks and tractable policies," *arXiv preprint arXiv:1804.05804*, 2018.

[15] P. Schulam and S. Saria, "Can you trust this prediction? auditing pointwise reliability after learning," in *The 22nd International Conference on Artificial Intelligence and Statistics*. PMLR, 2019, pp. 1022–1031.

[16] K. Verbert, B. De Schutter, and R. Babuška, "A multiple-model reliability prediction approach for condition-based maintenance," *IEEE Transactions on Reliability*, vol. 67, no. 3, pp. 1364–1376, 2018.

[17] S. Khaitan, Q. Lin, and J. M. Dolan, "Safe planning and control under uncertainty for self-driving," *IEEE Transactions on Vehicular Technology*, vol. 70, no. 10, pp. 9826–9837, 2021.

[18] H. Azpúrua, G. M. Freitas, D. G. Macharet, and M. F. Campos, "Multi-robot coverage path planning using hexagonal segmentation for geophysical surveys," *Robotica*, vol. 36, no. 8, pp. 1144–1166, 2018.

[19] W. Schwarting, J. Alonso-Mora, and D. Rus, "Planning and decision-making for autonomous vehicles," *Annual Review of Control, Robotics, and Autonomous Systems*, vol. 1, pp. 187–210, 2018.

[20] V. V. Petrov, "On lower bounds for tail probabilities," *Journal of statistical planning and inference*, vol. 137, no. 8, pp. 2703–2705, 2007.

[21] A. Wächter and L. T. Biegler, "On the implementation of an interior-point filter line-search algorithm for large-scale nonlinear programming," *Mathematical programming*, vol. 106, no. 1, pp. 25–57, 2006.

[22] R. Fourer, D. M. Gay, and B. W. Kernighan, "Ampl. a modeling language for mathematical programming," 2003.

[23] P. A. Ioannou and C.-C. Chien, "Autonomous intelligent cruise control," *IEEE Transactions on Vehicular technology*, vol. 42, no. 4, pp. 657–672, 1993.

[24] M. Hu, Y. Liao, W. Wang, G. Li, B. Cheng, and F. Chen, "Decision tree-based maneuver prediction for driver rear-end risk-avoidance behaviors in cut-in scenarios," *Journal of advanced transportation*, vol. 2017, 2017.

[25] B. Li, Z. Yin, Y. Ouyang, Y. Zhang, X. Zhong, and S. Tang, "Online trajectory replanning for sudden environmental changes during automated parking: A parallel stitching method," *IEEE Transactions on Intelligent Vehicles*, 2022.